HAL open science

Method to geometrically personalize a detailed finite element model of the spine

Nadine Lalonde, Yvan Petit, Carl-Eric Aubin, Eric Wagnac, Pierre-Jean Arnoux

To cite this version:

Nadine Lalonde, Yvan Petit, Carl-Eric Aubin, Eric Wagnac, Pierre-Jean Arnoux. Method to geometrically personalize a detailed finite element model of the spine. IEEE Transactions on Biomedical Engineering, 2013, 60 (7), pp.214-2021. 10.1109/TBME.2013.2246865 . hal-00865166

HAL Id: hal-00865166

https://hal.science/hal-00865166v1

Submitted on 24 Sep 2013

HAL is a multi-disciplinary open access archive for the deposit and dissemination of scientific research documents, whether they are published or not. The documents may come from teaching and research institutions in France or abroad, or from public or private research centers.

L'archive ouverte pluridisciplinaire **HAL**, est destinée au dépôt et à la diffusion de documents scientifiques de niveau recherche, publiés ou non, émanant des établissements d'enseignement et de recherche français ou étrangers, des laboratoires publics ou privés.

This article has been accepted for publication in a future issue of this journal, but has not been fully edited. Content may change prior to final publication.

TBME-01357-2012.R2

Method to geometrically personalize a detailed finite element model of the spine

Nadine M. Lalonde, Yvan Petit, Carl-Eric Aubin, Eric Wagnac, Pierre-Jean Arnoux

***Abstract*— To date, developing geometrically personalized and detailed solid finite element models of the spine remains a challenge, notably due to multiple articulations and complex geometries. To answer this problem, a methodology based on a free form deformation technique (kriging) was developed to deform a detailed reference finite element mesh of the spine (including discs and ligaments) to the patient-specific geometry of 10 and 82-year old asymptomatic spines. Different kriging configurations were tested: with or without smoothing, and control points on or surrounding the entire mesh. Based on the results, it is recommended to use surrounding control points and smoothing. The mean node to surface distance between the deformed and target geometries was 0.3 mm ± 1.1. Most elements met the mesh quality criteria (95%) after deformation, without interference at the articular facets. The method's novelty lies in the deformation of the entire spine at once, as opposed to deforming each vertebra separately, with surrounding control points and smoothing. This enables the transformation of reference vertebrae and soft tissues to obtain complete and personalized FEMs of the spine with minimal post-processing to optimize the mesh.**

***Index Terms*— Biomechanics, finite elements, kriging, spine**

I. Introduction

Finite element models of the spine have been used for several decades to evaluate their biomechanical response under different loadings or to evaluate corrective treatments, notably for scoliotic, osteoporotic or metastatic patients [1]-[3]. The complexity of the spine, due to multiple articulations and inter-individual variations in intricate vertebral shapes, makes it one of the most difficult structures to represent numerically.

Models can be geometrically parameterized [4]-[6], subject-specific [3], [7]-[10], or a combination of both [11]-[14]. The former can provide general information about pathology mechanisms or fracture risks, but not about personalized biomechanics.

Patient-specific models, based on multi-plane radiographic, computed tomography (CT) or magnetic resonance (MR) images, can be classified into three major categories: 1- beam models, 2- continuum-levelled models (or solid models), 3- micro-resolution models, which cannot be applied in vivo to the complete human spine [15], [16].

Beam models are easily obtained from stereoradiographic 3D reconstructions; automated algorithms have been developed to include discs and ligaments [3], [7], [10]. However, the simplified representation of the spine limits local analyses such as the interactions with surgical instruments and symptomatic bone regions.

Continuum models comprise automated CT voxel -based meshes [17] and meshes generated from stereoradiographic 3D reconstructed points or CT/MR contours [5], [12], [13], [19], [20]. Models derived from CT-scans or MR images generally require image segmentation, surface modelling and volume discretization, and are thus time consuming. A few automated mesh generation algorithms for CT-scans have been developed, such as landmark-based morphing [21], grid projection [8], [9], template-based generations [22], and voxel-based meshing [9], [23], [24]. Most studies usually concentrate on isolated vertebrae or spinal segments; furthermore, discs and ligaments are usually modelled during post-processing. To our knowledge, only Chui et al. [9] presented a CT-based continuum finite element mesh of the complete spine with discs, and personalized mechanical properties; however, the authors did not mention how they managed the intervertebral joints (discs, articular facets). High resolution continuum CT-voxel-based meshes are computationally expensive to solve and may present surface artefacts with insufficient boundary smoothing.

Free form deformation techniques, as dual kriging [25], [26] can be applied with 3D reconstructed points to deform detailed vertebral primitives and obtain surface or solid continuum meshes [12], [18], [27], [28]. Dual kriging is a linear unbiased estimator of a random function, and can be used as a general interpolation technique. The usual method consists in deforming (kriging) each vertebra separately based on control points placed on vertebral landmarks; an adjustment of each facet position must be performed to ensure articular coherence. Discs and ligaments are secondarily added. Local mesh distortions may appear at the control points if the

Manuscript received August 2012. This work was supported by the French Institute of Science and Technology for Transport, Development, and Networks (IFSTTAR).

N.M. Lalonde was with the Aix-Marseille Université, IFSTTAR, Université de la Méditerranée-Aix-Marseille, LBA, F-13916, Faculté de Médecine secteur Nord, Bd Pierre Dramard, 13916 Marseille (phone: +33 4 91 65 80 00; fax: +33 4 91 65 80 19; e-mail: nadine_michele_lalonde@hotmail.com).

Y Petit is with the Ecole de Technologie Supérieure of Montréal, 1100 Notre-Dame Ouest, Montréal, QC, H3C 1K3, Canada (e-mail yvan.petit@ets.ca).

CE Aubin is with Polytechnique Montreal, c.p. 6079 succ. Centre-Ville, Montréal, QC, H3C 3A7, Canada (e-mail carl-eric.aubin@polymtl.ca)

E Wagnac is with the Ecole de Technologie Supérieure de Montréal, 1100 Notre-Dame Ouest, Montréal, QC, H3C 1K3, Canada (e-mail eric.wagnac@polymtl.ca)

PJ Arnoux is with the Aix-Marseille Université, IFSTTAR, Université de la Méditerranée-Aix-Marseille, LBA, F-13916, Faculté de Médecine secteur Nord, Bd Pierre Dramard, 13916 Marseille (e-mail pierre-jean.arnoux@ifsttar.fr)

Copyright (c) 2013 IEEE. Personal use is permitted. For any other purposes, permission must be obtained from the IEEE by emailing pubs-permissions@ieee.org.

This article has been accepted for publication in a future issue of this journal, but has not been fully edited. Content may change prior to final publication.

primitive vertebra greatly differs from the target geometry.

The aim of the present study is to develop a methodology based on dual kriging to generate personalized solid finite element models of the complete spine (T1-L5) using a reference detailed model which includes discs and major ligaments, with minimal post-processing to ensure articular coherence and little mesh distortions. The method is to be compatible with different imaging techniques, such as CT-scan and X-ray reconstructions.

II. METHODS

Wagnac et al. [30] developed a detailed finite element model (FEM) of the spine (T1-S5) from the CT-scan images (thickness of 0.6 mm) of a young adult male with no known back problems (32 years old, weight of 75.5 kg, height of 1.75 m) [29], [30] (Fig. 1). The model was developed for the analysis of spinal trauma (ligament failure, bone fracture); its biomechanical behaviour was validated for the lumbar segment. It is presented here in its entire form. Each vertebra was composed of cancellous bone surrounded by a cortical shell modelled respectively by 4-nodes tetrahedrons and 3-nodes triangles, whose thickness varied according to their localisation on the vertebral body (total mesh size between 1 and 1.5 mm; shell thickness between 0.37 and 0.9 mm). Contact elements were added at the zygapophyseal processes. To take into account material inhomogeneity, several regions of cancellous and cortical bones were respectively created inside the vertebral body and on the vertebral endplates and attributed specific mechanical properties [**30**]. Intervertebral discs, composed of the annulus fibrosus and nucleus pulposus, were modelled with 5 layers of 8-nodes bricks. The annulus' collagenous fibers were represented by 8 layers of unidirectional springs organized in concentric lamellae with a crosswise pattern of approximately 35°. Principal spinal ligaments (from the sacrum to T10 vertebra) were modelled with 1-mm thick 3 or 4-nodes shell elements: anterior and posterior longitudinal ligaments (ALL and PLL), intertransverse ligaments (ITL), ligamentum flavum (LF), capsular ligaments (JC), interspinous ligaments (ISL), and supraspinous ligaments (SSL). Tied contact interfaces ensure the attachment of the discs and ligaments to the vertebrae. The model comprises 243,227 nodes and 1,029,782 elements. This model is referred to as the "source" FEM.

Two target spine geometric models (T1 to S5) were reconstructed from the CT-scan images of an isolated 82-year old female cadaver spine and of a 10-year old boy requiring CT-scan images for abdominal pain without spinal pathology, using the Mimics software (Materialise, Leuven, Belgium).

For both source and target reconstructed spines, 61 and 65 control points were respectively identified manually on the lumbar and thoracic vertebrae, for a total of 1085 points per spine (Fig. 2), using the Radioss software (Altair Engineering inc., Troy, MI, USA). Points were chosen to encompass each vertebra. Feasibility of kriging the sacrum was also tested by

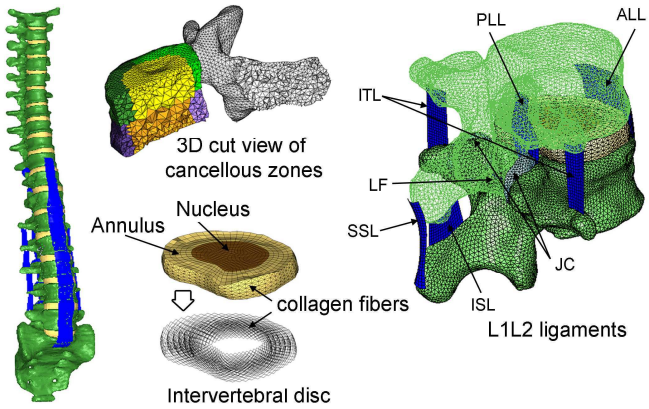

Fig. 1. Source finite element model, in surface and mesh representations

using a small sample of control points. Morphologic differences between the target and source sacrums explain this methodological choice: the 82-year old sacrum presented 5 dorsal foramina, compared to 4 in the child and source models.

As seen in certain morphing techniques [31], the source and target can be embedded in a generic shape. In this project, it was chosen to embed them with corresponding similar vertebral shapes, by applying a 3% scaling of the control points for each vertebra (source and target) about its vertebral body centre to obtain points surrounding the volume (Fig. 2). The two variants of control points were expressed as:

- K1: control points on the mesh
- K2: control points surrounding the mesh

Dual kriging was used to morph the detailed source FEM to the specific geometry of two different subjects, using the technique developed by Delorme et al. [27]. Based on the previous 1085 control points, a linear system representing the field of deformation between the initial and new coordinates was created and applied to all the nodes of the source model. Given the refinement of the source model, it was chosen to deform the entire spine, including the discs and ligaments, at once as opposed to deforming only each vertebra separately. Kriging was tested with and without a smoothing factor of -3 (or nugget effect [26]), for the two control point variants (K1 and K2), thus giving four kriging configurations: K1s0, K1s-3, K2s0, K2s-3. The smoothing value was chosen based on preliminary test not presented here.

The kriging equations in 3D were given by:

$$\begin{aligned} u(x) &= a_0^x + a_1^x x + a_2^x y + a_3^x z + \sum_{j=1}^{1085} b_j^x \left(\sqrt{(x-x_j)^2 + (y-y_j)^2 + (z-z_j)^2} \right) \\ u(y) &= a_0^y + a_1^y x + a_2^y y + a_3^y z + \sum_{j=1}^{1085} b_j^y \left(\sqrt{(x-x_j)^2 + (y-y_j)^2 + (z-z_j)^2} \right) \\ u(z) &= a_0^z + a_1^z x + a_2^z y + a_3^z z + \sum_{j=1}^{1085} b_j^z \left(\sqrt{(x-x_j)^2 + (y-y_j)^2 + (z-z_j)^2} \right) \end{aligned} \quad (1)$$

where

- u(x,y,z) : new coordinates of an arbitrary model node
- x, y, z : initial coordinates of the arbitrary model node
- x_j, y_j, z_j : coordinates of the source control points

Copyright (c) 2013 IEEE. Personal use is permitted. For any other purposes, permission must be obtained from the IEEE by emailing pubs-permissions@ieee.org.

This article has been accepted for publication in a future issue of this journal, but has not been fully edited. Content may change prior to final publication.

- coefficients a_0, a_1, a_2, a_3 and b_j are solutions of the following system defined by the *1085* control points:

$$\begin{bmatrix} & & & 1 & x_1 & y_1 & z_1 \\ & k(h) & & \vdots & \vdots & \vdots & \vdots \\ & & & 1 & x_{1085} & y_{1085} & z_{1085} \\ 1 & \cdots & 1 & 0 & 0 & 0 & 0 \\ x_1 & \cdots & x_{1085} & 0 & 0 & 0 & 0 \\ y_1 & \cdots & y_{1085} & 0 & 0 & 0 & 0 \\ z_1 & \cdots & z_{1085} & 0 & 0 & 0 & 0 \end{bmatrix} \begin{bmatrix} b_1^x & b_1^x & b_1^x \\ \vdots & \vdots & \vdots \\ b_{1085}^x & b_{1085}^x & b_{1085}^x \\ a_0^x & a_0^x & a_0^x \\ a_1^x & a_1^y & a_1^z \\ a_2^x & a_2^y & a_2^z \\ a_3^x & a_3^y & a_3^z \end{bmatrix} = \begin{bmatrix} u_1^x & u_1^y & u_1^z \\ \vdots & \vdots & \vdots \\ u_{1085}^x & u_{1085n}^x & u_{1085}^x \\ 0 & 0 & 0 \\ 0 & 0 & 0 \\ 0 & 0 & 0 \\ 0 & 0 & 0 \end{bmatrix} \quad (2)$$

where

- $u_j^{x,y,z}$: coordinates of the target control points
- x_i, y_i, z_i : coordinates of the source control points

k(h) is expressed as:

$$k(h) = \begin{bmatrix} k(0)+\sigma & \cdots & k(|x_1 - x_{1085}|) \\ \vdots & \ddots & \vdots \\ k(|x_{1085n} - x_1|) & \cdots & k(0)+\sigma \end{bmatrix} \quad (3)$$

where σ is the smoothing factor

Validation of the deformed model was performed by 1- a general appreciation of the deformed spine to identify mesh incoherence such as excessive deformations (mesh peaks to reach the control points) and mesh auto-penetration (mesh folding), 2- calculating the target and source control point distance after kriging, to measure the smoothing effect, 3- evaluating the node to surface distances between each deformed source and corresponding target vertebrae with the CATIA software (Dassault Systems, Vélizy Villacoublay, France), and 4- verifying mesh quality criteria [32], such as:

- Jacobian: ratio between the smallest and largest determinants of the Jacobian matrix for each element integration point;
- Warping: each quadrilateral element was divided into two triangles along its diagonal, and warping was calculated as the angle between the triangles' normal;
- Aspect ratio: longest edge length divided by shortest edge length for each 2D element and each face of 3D elements;
- Volume aspect ratio: longest edge length divided by the shortest height for tetrahedral elements or the shortest edge length for hexahedral elements;
- Skew: for 2D triangular elements, minimum angle (0-90°) between the vector from each node to the opposite edge and the mid-vector between the two adjacent sides;
- Volume skew: for tetrahedral elements, ratio between the element's true volume by the volume of a hypothetical perfect equilateral element of the same circumradius (radius of a sphere passing through the four vertices of the element).

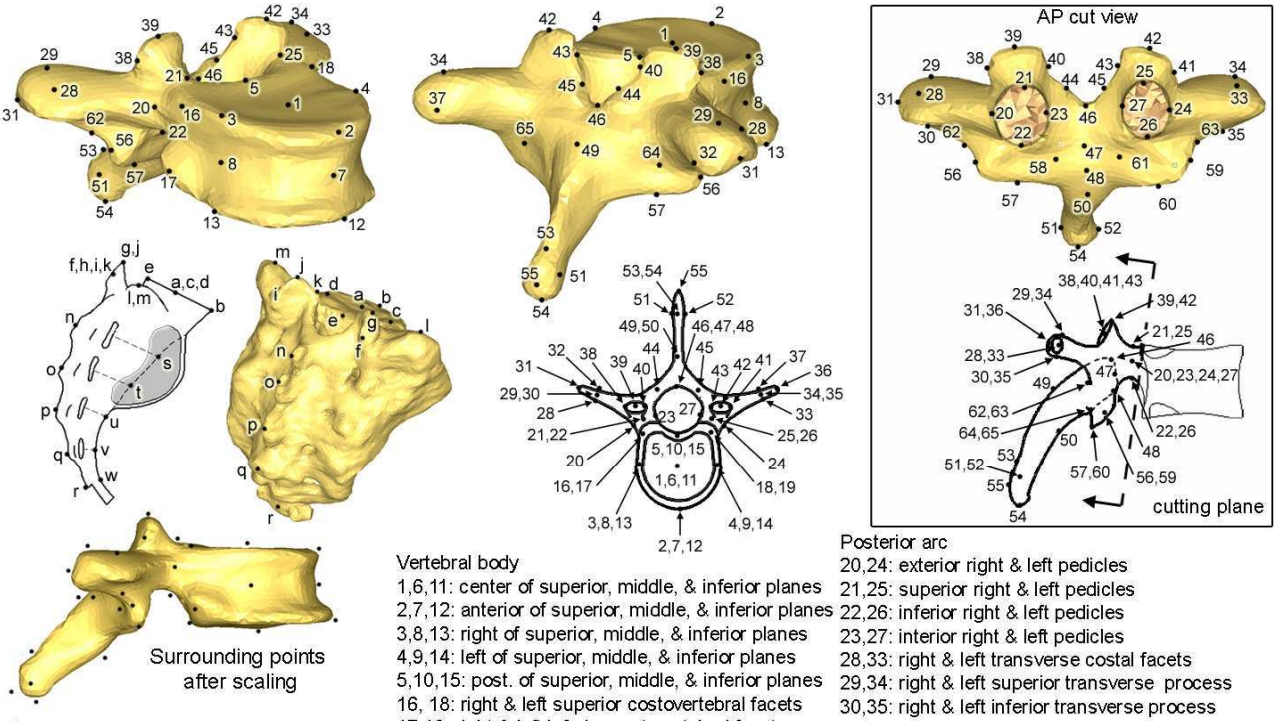

Sacrum
a -e: center, ant., right, left, & post. S1 plate
f,i: right & left exterior of facets
g,j: right & left apex of facets
h,k: right & left interior of facets
l,m: right & left apex of sacral ala
n-q: S1-S4 sipous tubercles
r: posterior S5
s-w: S1-S5 transverse ridges

Vertebral body
1,6,11: center of superior, middle, & inferior planes
2,7,12: anterior of superior, middle, & inferior planes
3,8,13: right of superior, middle, & inferior planes
4,9,14: left of superior, middle, & inferior planes
5,10,15: post. of superior, middle, & inferior planes
16, 18: right & left superior costovertebral facets
17,19: right & left inferior costovertebral facets
Articular facets
38,41: right & left exterior of superior facets
39,42: right & left apex of superior facets
40,43: right & left interior of superior facets
56,59: right & left exterior of inferior facets
57,60: right & left apex of inferior facets
58,61: right & left interior of inferior facets
64,65: right & left posterior point of inferior facets

Posterior arc
20,24: exterior right & left pedicles
21,25: superior right & left pedicles
22,26: inferior right & left pedicles
23,27: interior right & left pedicles
28,33: right & left transverse costal facets
29,34: right & left superior transverse process
30,35: right & left inferior transverse process
31,36: right & left extremity of transverse process
32,37: right & left posterior transverse process
44,45: right & left superior pars
62,63: right & left inferior pars
46,47,48: sup., middle, & inf. points of post. wall
49,50: sup. & inf. of spinous process on the lamina
51,52; right & left spinous process extremety
53,54: sup. & inf. of spinous process extremety
55: extremety of spinous process

Fig. 2. Vertebral and sacral control points

Copyright (c) 2013 IEEE. Personal use is permitted. For any other purposes, permission must be obtained from the IEEE by emailing pubs-permissions@ieee.org.

This article has been accepted for publication in a future issue of this journal, but has not been fully edited. Content may change prior to final publication.

III. RESULTS

General appreciation of the deformed models revealed that the best transformations were obtained when control points surrounded the vertebrae and with the use of the smoothing factor (K2s-3 configuration), whereas the other configurations produced local mesh distortions (peaks, folding). Typical examples of kriged vertebrae are shown in Fig. 3 for both targets (T4 for the child spine, L2 for the elderly spine) according to the different kriging configurations. Control points located directly on the mesh without smoothing (K1s0) produced local peaks on the vertebral body and on the articular facets, as well as mesh folding interferences on a few vertebrae for both models (child and elderly). Smoothing (K1s-3) minimized these mesh distortions, mainly for the child spine (Fig. 3). Kriging with control points not directly on the mesh without smoothing (K2s0) diminished the mesh peaks for the elderly spine, but did not prevent the auto-mesh penetration for the child spine.

for the elderly spine, but did not prevent the auto-mesh penetration for the child spine.

Fig. 4 presents the kriged spines for the two target geometries with the K2s-3 configuration, in surface mode for clarity. It can be seen that for both models, the deformed spine matches adequately the target general shape, with also proper transformation of the discs and ligaments. However, differences on the vertebral endplate shapes were noted for the child target (Fig. 4 a), which were more rounded in the original reconstructed child spine and more convex on the deformed spine.

The distance between the control points before and after kriging was calculated for each configuration. No difference was found between the control points after transformation for configuration K1 without smoothing (K1s0). Using smoothing with the points on the mesh (K1s-3) resulted in mean differences between the control points of 0.7 and 0.9 mm and

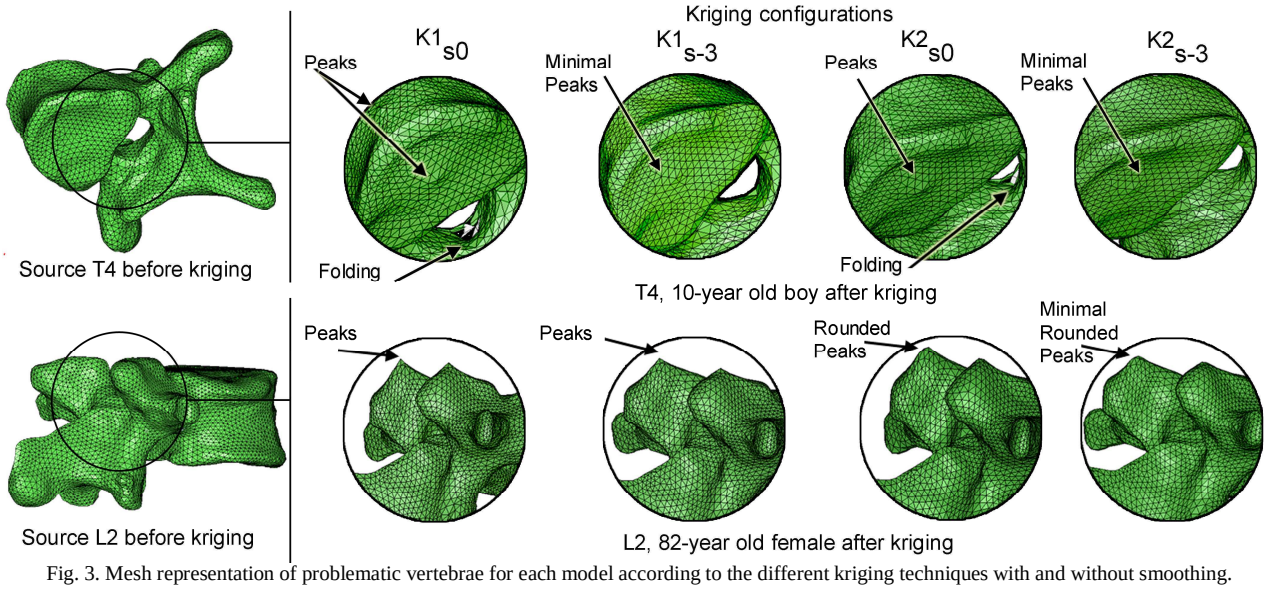

Fig. 3. Mesh representation of problematic vertebrae for each model according to the different kriging techniques with and without smoothing.

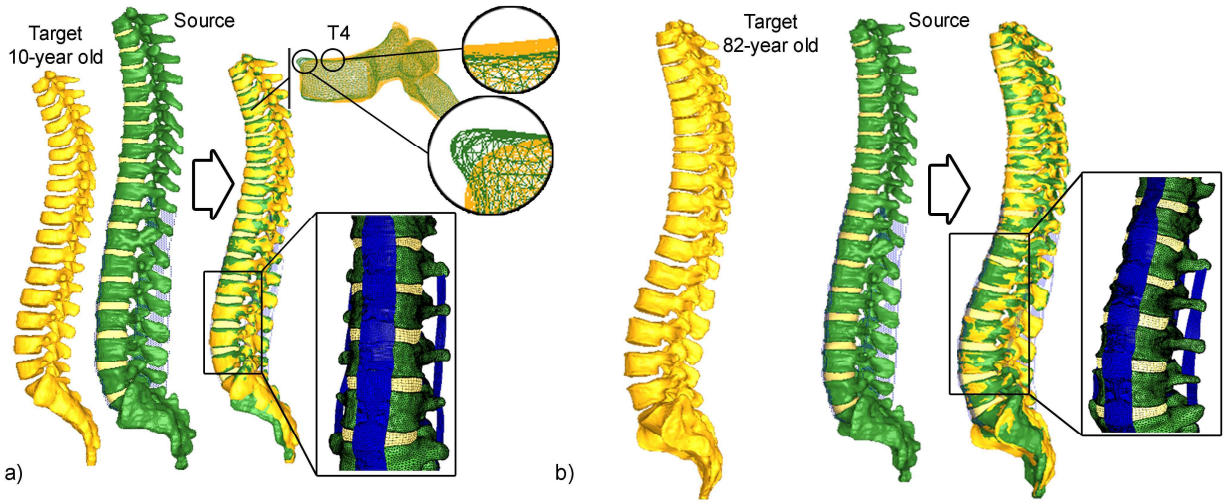

Fig. 4. Surface representation of spine models before and after kriging with the K2s-3 configuration: a) 10-year old boy target, with mesh representation and vertebral body discrepancies for T4 vertebra, b) 82-year old female target, with mesh representation.

Copyright (c) 2013 IEEE. Personal use is permitted. For any other purposes, permission must be obtained from the IEEE by emailing pubs-permissions@ieee.org.

This article has been accepted for publication in a future issue of this journal, but has not been fully edited. Content may change prior to final publication.

maximum differences of 2.8 and 4.2 mm for the child and elderly spines respectively. Using control points surrounding the mesh without smoothing (K2s0) had less influence on the final control point distances than the K1s-3 configuration, with mean values of 0.3 mm and 0.5 mm for the child and elderly spines (maximum values of 2.0 and 2.7 mm). A greater increase in mean (1.2 mm) and maximum (5.0 mm) control point distances was obtained with the surrounding control points and smoothing (K2s-3).

The node to surface distances between the deformed mesh and the target model showed little variations despite the four kriging configurations, with overall signed mean differences under or equal to 0.3 mm (standard deviation 1.2 mm) and maximum values of 5.2 mm for the child spine and 6.4 mm for the elderly spine. Fig. 5 shows the node to surface distances with color scaling between the kriged source model and the targets for configuration K2s-3. For the child spine, 96% of the node to surface distances were within 2 mm, compared to 91% for the elderly spine. Greater differences were notably noticed at the vertebral endplates for the child and at the articular facets for the 82-years old spine. Node to surface distances were higher for the sacrum: 0.5 ± 2.7 mm (max 9.5) and -0.1 ± 3.3 mm (max 13.1) for the 10 and 82-year old spines respectively. The highest differences were located in extrapolated regions, notably on the lateral parts of the sacrum where no control points were positioned.

Mesh quality criteria are given in Table I for the K2s-3 configuration, which showed the least mesh distortions. Most elements met the initial model criteria, with only small increases in percentage of failed elements for the vertebra volume aspect ratio (from 0% to 1% failed) and for the disc warping (from 2% to 3% failed). The largest increase in failed elements was noted for the vertebrae volume skew criteria which increased by 6%. Both spines had similar criteria changes despite their different vertebral shapes and global postural curvatures. Overall, 95% of the elements met the quality criteria.

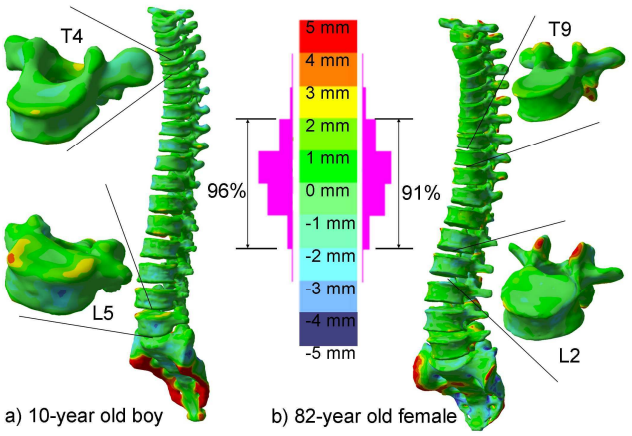

Fig. 5. Node to surface distances after kriging for configuration K2s-3 for both targets.

Table I. Mesh quality criteria with % of failed elements per anatomical structure for configuration K2s-3.

	Initial model	Kriged 82-year old	Kriged 10-year old
Vertebrae 2D elements (n = 192 867 trias)			
Aspect ratio	0%	0%	0%
Skew	0%	0%	0%
Jacobian	0%	0%	0%
Vertebrae 3D elements (n = 726 379 tetras)			
Aspect ratio	0%	0%	0%
Skew	0%	**1%**	**1%**
Jacobian	0%	0%	0%
Vol skew	1%	**7%**	**7%**
Vol aspect ratio	0%	**1%**	**1%**
Ligaments 2D elements (n = 7 793 trias, 13 473 quads)			
Warping	1%	1%	1%
Aspect ratio	0%	0%	0%
Skew	0%	0%	0%
Jacobian	0%	0%	0%
Discs 3D elements (n = 40 250 hexas)			
Warping	2%	**3%**	**3%**
Aspect ratio	0%	0%	0%
Skew	0%	0%	0%
Jacobian	5%	5%	5%
Vol aspect ratio	0%	0%	0%

IV. DISCUSSION

This study has shown that the free form kriging deformation technique can be used to geometrically personalize a detailed solid finite element model of the spine, initially developed for general accidentology and biomedical evaluations, despite the great differences in geometry and posture with the two target spines.

To the authors' knowledge, only Chui et al. [9] presented a personalized continuum spinal finite element model with discs based on ct-scan images. However, such models are computational expensive with high resolution (higher number of elements) and do not comprise other structures such as ligaments.

As opposed to contours extracted from CT or MRI-based images, the present method is based on control points, and is thus compatible with other imaging techniques generating such data, notably X-ray reconstructions, frequently used with scoliotic patients [3], [10]. However, the accuracy of the method to generate personalized and detailed models still needs to be tested with such complex spinal curvatures.

Control points were identified manually by one operator on the CT images, which was time consuming (4-5 hours per spine). The intra-observer variability was tested for a few vertebrae and was under 3 mm. Semi-automated control point identifications techniques should be developed when using body scan images. Such techniques are notably used with X-ray images [33]. Automated techniques would reduce the intra- and inter-operator variability. Depending on the use and analysis to be done with the personalized model, proper control point positioning is recommended, as greater reconstruction differences with the real spine could affect its simulated mechanical behaviour.

Copyright (c) 2013 IEEE. Personal use is permitted. For any other purposes, permission must be obtained from the IEEE by emailing pubs-permissions@ieee.org.

This article has been accepted for publication in a future issue of this journal, but has not been fully edited. Content may change prior to final publication.

Kriging was performed on the entire spine at once, as opposed to kriging each vertebra separately [3], [7], [18], [27], [28] in order to prevent interference at the articular facets. Other studies adjust the articular facets during post-processing. Aubin et al. [7] reported mean errors of 3.8 mm for the tips of the articular facets when using kriging with target points obtained from 3D X-ray reconstructions, but with the pair of adjoining articular facets perfectly parallel.

Kriging the whole spine at once also enabled the direct transformation of discs and ligaments already included in the source model, reducing the need for post-processing. Kriging the spine at once will also facilitate further modelling developments, such as the incorporation of other ligaments and the rib cage, since this only needs to be brought to the source model which will be deformed as a whole entity as opposed to deforming each structure separately.

The use of a smoothing factor in the kriging formula or the use of surrounding control points both produced mesh smoothing, but at different degrees for the child and elderly spines. Surrounding control points alone did not prevent mesh foldings in child vertebrae. The combination of both techniques (K2s-3) produced the best results, and minimized the local mesh distortions which could be seen with the other kriging configurations tested as well as in previous studies based on kriging. Smoothing or surrounding points influenced the control point precision, but did not affect the overall node to surface distances, with mean values less than 0.5 mm, which is in the range of the accuracy of the reconstructed target models (Mimics software, Materialise, Leuven, Belgium).

When the target and source geometries greatly differ locally, mesh distortions appear after kriging. This was noticed at the center of the child endplates and at the articular facets of the L2 elderly vertebra, which were proportionally bigger and more round than the source. These distortions, which were independent of the kriging configuration, reflect a limit of the method when the target and source differ locally.

Compared to adults, child vertebrae are typically domed due to the presence of the vertebral growth plates; the apophyseal ring, which produces the typical convex adult endplates, is absent [34], [35]. As the source model was built from an adult spine, kriging it into a child geometry could not reproduce this youth characteristic. The deformed source vertebrae maintained their original shapes, such as the outer curvature brought by the apophyseal ring and the convex curve in the center of the vertebral endplates. Hence, the greatest node to surface distance was located on the vertebral endplates. If personalized child spine modelling is desired, it is recommended to use a pediatric source model, which incorporates the vertebral growth plates thus generating the domed vertebral endplate shape.

Most elements (95%) met the mesh quality criteria after kriging, compared to 99% before transformation. Volume skew was the most affected mesh quality criteria for both target models. This may be explained by the squeezing or stretching of vertebral zones resulting from kriging, depending on the control point locations. Optimizing the source model to avoid initial failed elements may reduce the number of failed elements after kriging. Mesh quality should always be checked, specifically in critical anatomical regions that can affect the overall structural biomechanics of the model, such as the disks or ligaments. Local mesh refinement can be done during post-treatment to rectify the problematic elements that do not meet the mesh quality criteria.

Another limit to the proposed approach of free form deformation to geometrically personalize finite element models of the spine lies in the fact that the target geometry must be compatible with the source model, and have 12 thoracic vertebrae, 5 lumbar vertebrae, and 5 sacral vertebrae. In this study, the child and source sacrum presented 5 sacral vertebrae, compared to 6 in the elderly spine. Hence, only the feasibility of kriging this structure was tested by using with a few control points positioned mostly along the medial sacral plane, on S1 endplate and on the articular facets. As expected, less accuracy was obtained on the outermost aspect of the sacrum. The determination of proper control points for this structure still needs to be investigated.

To date the reference model, which has been under construction for more than 5 years, has been developed from T1 to the sacrum and has been validated under different mechanical loadings and speeds against published and experimental data for the T12-L5 segment [30]. Complete understanding of the effect of the proposed geometrical personalization on the model's overall mechanical behaviour in static and dynamic conditions still needs to be addressed, in relation with the chosen control points. Personalization of mechanical properties is another important field of interest which still needs to be answered. The proposed work represents a compromise between 100% geometrically personalized models based on scan images, which are time consuming, and lesser personalized but more automated models used with other imaging techniques such as planar radiographs.

This method is one of the few that enables the generation of complete personalized solid spinal models including discs, ligaments, and articular facets. Based on our results, it is recommended to deform the entire spine at once using surrounding control points and a small smoothing factor. Personalized models could notably be used to develop pre-operative strategies.

Copyright (c) 2013 IEEE. Personal use is permitted. For any other purposes, permission must be obtained from the IEEE by emailing pubs-permissions@ieee.org.

This article has been accepted for publication in a future issue of this journal, but has not been fully edited. Content may change prior to final publication.

ACKNOWLEDGMENT

This work was founded by the French institute of science and technology for transport, development and networks (IFSTTAR).

REFERENCES

[1] A. Shirazi-Adl, A.M. Ahmed, S.C., and Shrivastava, "A finite element study of a lumbar motion segment subjected to pure sagittal plane moments," *J. Biomech*., vol 19, no. 4: pp. 331-350, 1986.

[2] V.K. Goel and L.G. Gilbertson, "Applications of the finite element method to thoracolumbar spinal research – past, present, and future," *Spine*, vol. 20, no. 15, pp. 1719-1727, 1995.

[3] C.E. Aubin, J.L. Descrimes, J. Dansereau, W. Skalli, F. Lavaste, and H. Labelle, "Geometrical modeling of the spine and the thorax for the biomechanical analysis of scoliotic deformities using the finite element method," *Ann Chir*, vol. 49, no. 8, pp. 749-61, 1995.

[4] F. Galbusera, C.M. Bellini, H.N. Aziz, M.T. Raimondi, M. Brayda-Bruno, and M. Fornari, "Parametric FE mesh generation: application to the cervical spine," *J Applied Biomat & Biomech*, vol. 6, no. 2, pp. 95-103, 2008.

[5] M. Driscoll, C.E. Aubin, A. Moreau, I. Villemure, and S. Parent, "The role of spinal concave-convec biases in the progression of idiopathic scoliosis," *Eur Spine J*, vol. 18, pp.180-187, 2009.

[6] G.J.M. Meijer, J. Homminga, E.E.G. Hekman, A.G. Veldhuizen, and G.J. Verkerke, "The effect of three-dimensional geometrical changes during adolescent growth on the biomechanics of a spinal motion segment," *J Biomech*, vol. 43, pp.1590-1597, 2010.

[7] C.E. Aubin, J. Dansereau, F. Parent, H. Labelle, and J.A. de Guise, "Morphometric evaluations of personalised 3D reconstructions and geometric models of the human spine," *Med & Biol Eng & Comput*, pp. 611-618, nov. 1997.

[8] J.C.M. Teo, C.K. Chui, Z.L. Wang, S.H. Ong, C.H. Yan, S.C. Wang, H.K. Wong, and S.H. Teoh, "Heterogenous meshing and biomechanical modelling of human spine," *Med Eng & Physics*, vol. 29, pp. 277-290, 2007.

[9] C.K. Chui, Z. Wang, J. Zhang, J.S.K. Ong, L. Bian, J.C.M. Teo, C.H. Yan, S.H. Ong, S.C. Wang, H.K. Wong, and S.H. Teoh, "A component-oriented software toolkit for patient-specific finite element model generation," *Advances in Engineering Software*, vol. 40, pp.184-192, 2009.

[10] J. Clin, C.E. Aubin, S. Parent, and H. Labelle, "A biomechanical study of the Charleston brace for the treatment of scoliosis," *Spine*, vol. 35, no. 19, pp. E940-947, 2010.

[11] F. Lavaste, W. Skalli, S. Robin, R. Roy-Camille, and C. Mazel, "Three-dimensional geometrical and mechanical modelling of the lumbar spine," *J Biomech*, vol. 25, no. 10, pp. 1153-1164, 1992.

[12] A. Laville, S. Laporte, and W. Skalli, "Parametric and subject-specific finite element modelling of the lower cervical spine-Influence of geometrical parameters on the motion patterns," *J Biomech*, vol. 42, pp. 1409-1415, 2009.

[13] N.M. Lalonde, I. Villemure, R. Pannetier, S. Parent, and C.E. Aubin, "Biomechanical modeling of the lateral decubitus posture during corrective scoliosis surgery," *Clin Biomech*, vol; 25, no. 6, pp. 510-516, 2010.

[14] E. Sapin, E. Jolivet, D. Mitton, and W. Skalli, "Prediction of the vertebral strength using a subject-specific finite-element model," *Compt Methods Biomech Biomed Eng*, vol. 12, suppl. S1, pp. 225-226, 2009.

[15] S.K. Eswaran, A.J. Fields, P. Nagarathnam, and T.M. Keaveny, "Multi-scale modelling of the human vertebral body: comparison of micro-ct based high-resolution and continuum-level models," *Pacific Symp Biocomput*, vol. 14, pp. 293-303, 2009.

[16] D.H. Pahr and P.K. Zysset, "From high-resolution ct data to finite element models; development of an integrated modular framework," *Comput Methods Biomech & Biomed Eng*, vol. 12, no. 1, pp. 45-57, 2009.

[17] R.P. Crawford, C.E. Cann, and T.M. Keaveny, "Finite element models predict in vitro vertebral body compressive strength better than quantitative computed tomography," *Bone*, vol. 33, pp. 744-750, 2003.

[18] P.L. Sylvestre, I. Villemure, and C.E. Aubin, "Finite element modeling of the growth plate in a detailed spine model," *Med Biol Eng Comput*, vol. 45, pp. 977-988, 2007.

[19] J.P. Little and C.J. Adam, "The effect of soft tissue properties on spinal flexibility in scoliosis : biomechanical simulation of fulcrum bending," *Spine*, vol. 34, no. 2, pp. E76-82, 2009.

[20] D. Tawara, J. Sakamoto, H. Murakami, N. Kawahara, J. Oda, and K. Tomita, "Mechanical evaluation by patient-specific finite element analyses demonstrates therapeutic effects for oeteoporotic vertebrae," *J Mechanial Behavior of Biomedical Materials*, vol. 3, pp. 31-40, 2010.

[21] M.A. O'Reilly and C.M. Whyne, "Comparison of computed tomography based parametric and patient-specific finite element models of the healthy and metastatic spine using a mesh-morphing algorithm," *Spine*, vol. 33, no. 17, pp. 1876-1881, 2008.

[22] L. Baghdadi, D.A. Steinman, and H.M. Ladak, "Template-based finite-element mesh generation from medical images," *Comput Med & Prog Biomedicine*, vol. 77, pp. 11-21, 2005.

[23] D.L. Camacho, R.H. Hopper, G.M. Lin, and B.S. Myers, "An improved method for finite element mesh generation of geometrically complex structures with application to the skullbase," *J Biomech*, vol. 30, no.10, pp. 1067-70, 1997.

[24] Z.L. Wang, J.C.M. Teo, C.K. Chui, S.H. Ong, C.H. Yan, S.C. Wang, H.K. Wong, and S.H. Teoh, "Computational biomechanical modelling of the lumbar spine using marching-cubes surface smoothened finite element voxel meshing," *Comput Methods & Prog Biomedicine*, vol. 80, pp. 25-35, 2005.

[25] M.R. Stytz and R.W. Parrott, "Using kriging for 3D medical imaging," *Comput Med Imaging & Graphics*, vol. 17, no. 6, pp. 421-442, nov.-dec. 1993.

[26] F. Trochu, "A contouring program based on dual kriging interpolation," *Eng with computers*, vol. 9, pp. 160-177, 1993.

[27] S. Delorme, Y. Petit, J.A. de Guise, H. Labelle, C.E. Aubin, and J. Dansereau, "Assessment of the 3-D reconstruction and high-resolution geometrical modeling of the human skeletal trunk from 2-D radiographic images," *IEEE Tr Biomed Eng*, vol. 50, no. 8, pp. 989-98, 2003.

[28] T. Serre, K. Bruyere, D. Mitton, T. Bekkour, S. Bertrand, J.P. Verriest, W. Skalli, K. Kayvantash, and C. Brunet, "Humos (Human model for safety) geometry : from one specimen to the 5th and 95th percentile," *SAE Transaction, Journal of passengers cars: mechanical systems*, paper 2006-01-2324, pp. 1660-1669, 2006.

[29] M. El-Rich, P.J. Arnoux, E. Wagnac, C. Brunet, and C.E. Aubin, "Finite element investigation of the loading rate effect on the spinal load-sharing changes under impact conditions," *J Biomech*, vol. 42, pp. 1252-1262, 2009.

[30] E. Wagnac, P.J. Arnoux, A. Garo, and C.E. Aubin, "Finite element analysis of the influence of loading rate on a model of the full lumbar spine under dynamic loading conditions," *Med Biol Eng Comput.*, vol. 50, pp. 903-915, 2012.

[31] J. Xiaogang, W. Huagen, and P. Qunsheng, "Geometric deformations based on 3D volume morphing," *J Comput Sci & Technol*, vol. 16, no. 5, pp. 443-449, 2001.

[32] P.J. Frey and P.L. George, "Maillage: application aux elements finis, " Paris : Hermes Science, 840p., 1999.

[33] S. Kadoury, F. Cheriet, C. Laporte, and H. Labelle, "A versatile 3D reconstruction system of the spine and pelvis for clinical assessment of spinal deformities, " *Med Bio Eng Comput*, vol. 45, pp. 591-602, 2007.

[34] J.R. Taylor, "Growth of human intervertebral discs and vertebral bodies," *J Anat*, vol. 120, no. 1, pp. 49-68, 1975.

[35] A. Dimeglio and F. Bonnel, "Le rachis en croissance : scoliose, taille assise et puberté, " Paris : Springer-Verlag, pp. 21-80., 1990.

Copyright (c) 2013 IEEE. Personal use is permitted. For any other purposes, permission must be obtained from the IEEE by emailing pubs-permissions@ieee.org.

This article has been accepted for publication in a future issue of this journal, but has not been fully edited. Content may change prior to final publication.

Nadine Michèle Lalonde obtained the Ph.D. degree in biomedical engineering in 2005, at Ecole Polytechnique of Montréal, Canada. She completed two years of fellowship also at the Ecole Polytechnique, where she developed a simplified personalized finite element model of the adolescent spine to study new minimally invasive treatments for scoliotic patients. She recently finished a second fellowship at the IFSTTAR research institute.

Her research interests are related to youth spinal finite element models for applications in trauma and surgical treatments.

Yvan Petit was born in Montreal, QC, Canada, in 1964. He received the B.Eng and M.A.Sc.degrees in mechanical engineering and the Ph.D. degree in biomedical engineering from ÉcolePolytechnique, Montreal, in 1992, 1995 and 2003, respectively.

He is currently Associate Professor at the Mechanical Engineering Department of École de technologiesupérieure, Montreal, QC, Canada. He is also Researcher and Head of the trauma group at Hôpital du Sacré-Coeur de Montréal. His current research interests include biomechanics, 3D geometrical and biomechanical modeling of the musculoskeletal, spinal trauma and design of medical devices.

Carl-Eric Aubin Ph.D., P.Eng. is Full Professor at Polytechnique Montreal in the Department of Mechanical Engineering and the Biomedical Engineering Institute, and Researcher at the Research Center of Sainte Justine University Hospital Center. He received the B.Eng. (1991) and the Ph.D. (1995) degrees in mechanical engineering (biomechanics) from Polytechnique Montreal. He is NSERC-Medtronic Industrial Research Chair in Spine Biomechanics and Polytechnique Excellence Research Chair in Orthopedic Engineering. His research interests include orthopedic biomechanics, 3D reconstruction and geometrical modeling of the spine, finite element modeling, spine surgery simulations, pathomechanisms of spinal deformities, and design of biomedical technologies. He is Fellow of the Scoliosis Research Society, Board Member of the International Research Society of Spinal Deformities, Past-President of the Quebec Scoliosis Society, Founding member of Computer Assisted Orthopedic Surgery International.

Eric Wagnac received the B.Eng and M.Sc.A degrees from Polytechnique Montreal, QC, Canada, in mechanical and biomedical engineering in 2002. He obtained the Ph.D. degree in biomedical engineering with codiplomation from Aix-Marseille University, France, and Polytechnique Montreal, QC, Canada, in 2011.

He held a Research Assistant position at the Canada Research Chairs «CAD Innovation in Orthopedic Engineering» at Ecole Polytechnique of Montreal between 2005 and 2006. He also held a Project Engineer position at Sinlab Biostructures Inc., Boisbriand, QC, Canada, between 2002 and 2005. Since 2011, he is working as a Postdoctoral Research Fellow at École de technologie superieure, Montreal, QC, Canada. His current and previous research works focus on spine biomechanics and computer modeling with biomechanical applications such as spinal trauma, rehabilitation engineering and design of surgical instrumentation and protection devices.

Pierre-Jean Arnoux With an initial background in applied mathematics, Pierre Jean Arnoux, worked on solid mechanics and came to biomechanics during its PhD dissertation "Modelling of knee ligaments" performed jointly at INRETS and CNRS Marseille (1996-2000). He joined the Mecalog Safety Business Unit (2000-2002) to work on biomechanics and biomedical applications with activities related to the design and validation of human and dummy model. Researcher at IFSTTAR (previously named INRETS) since 2002, he is now the executive manager of the "Laboratoire de BiomécaniqueAppliquée" which is a joint research Unit depending from IFSTTAR and Aix Marseille University. Its mains activities are related to the design and validation of finite element modelling of the human body; Injury mechanisms and virtual trauma investigation through FE simulation and mechanical behaviour of biological tissues coupling experimental and theoretical features.

Copyright (c) 2013 IEEE. Personal use is permitted. For any other purposes, permission must be obtained from the IEEE by emailing pubs-permissions@ieee.org.